PHYSICAL REVIEW A VOLUME 24, NUMBER 1 JULY 1981

Four-wave parametric interactions in a strongly driven two-level system

Robert W. Boyd, Michael G. Raymer, Paul Narum,* and Donald J. Harter
The Institute of Optics, University of Rochester, Rochester, New York 14627
(Received 25 September 1980)

We present an analysis of four-wave parametric amplification resulting from the nonlinear response of a two-level atomic system. The atomic dipole moment induced by weak optical fields at frequencies ω_3 and ω_4 in the presence of an optical field of arbitrary intensity at frequency ω_1, where $\omega_3+\omega_4=2\omega_1$, is obtained by solving the density-matrix equations of motion with phenomenological damping constants. The resulting nonlinear polarization can induce loss or three-photon gain in either weak wave and can act to parametrically couple these waves. The spatial evolution of the weak-field amplitudes is obtained by finding approximate solutions to the Helmholtz wave equations using the nonlinear polarization for the source terms. These solutions predict large gain for either or both of the weak waves under experimentally attainable conditions. Depending on the circumstance, this gain can be attributed solely to the three-photon gain, solely to the parametric coupling, or to an interplay between these effects. In addition, the solutions show an enhancement in the gain when $|\omega_3-\omega_1|=|\omega_4-\omega_1|=\Omega'$, where Ω' is the generalized Rabi frequency associated with the driving of the atoms by the wave at frequency ω_1.

I. INTRODUCTION

This paper discusses the four-wave parametric interactions which occur when nearly copropagating electromagnetic waves at three distinct frequencies interact in a two-level atomic vapor. It is assumed that two of the waves have weak amplitudes while the amplitude of the third wave is arbitrarily large. It is found that this four-wave mixing process can lead to parametric amplification of the weak waves and can thus lead to the generation of tunable radiation. We show that strong, previously unrecognized resonances occur in the gain profile at frequencies symmetrically displaced from that of the driving laser by the generalized Rabi frequency, and further that the positions of these resonances may be tuned by changing the intensity of the driving laser.

The process of four-wave parametric amplification and oscillation was treated theoretically by Chiao *et al.*[1] in 1966 for the case of waves interacting through a real $\chi^{(3)}$ susceptibility, and degenerate four-wave parameteric amplification was observed in CS_2 by Carman *et al.*[2] soon thereafter. Pellin and Yardley[3] have discussed the possibility of four-wave parametric oscillation utilizing the resonantly enhanced, nonlinear response of a multilevel atomic system in the limit where saturation effects and ac Stark shifts can be neglected. Parametric amplification utilizing the nonlinear response of a two-level atomic system to an exactly resonant pump field has been treated by Mollow.[4]

The parametric amplification process that we discuss here is closely related to that of four-wave mixing of two counterpropagating or nearly counterpropagating pump waves with two counterpropagating or nearly counterpropagating weak waves. This process also shows gain and can be used for the generation of phase-conjugate waves,[5] but it differs from the process considered here in that the gain is not exponential and in that interference of the pump waves leads to a spatial modulation of the pump intensity which significantly alters the nature of the interaction. Theoretical treatments of four-wave mixing in a two-level system for the case of nearly counterpropagating pump waves have been presented by Abrams and Lind[6] for degenerate mixing for the case of arbitrarily strong pump waves, by Nilsen and Yariv[7] for nondegenerate mixing in the limit where the pump waves are sufficiently weak that the atomic response can be calculated using third-order time-dependent perturbation theory, and by Fu and Sargent[8] and Harter and Boyd[9] (whose methodology is similar to that of the present paper) for the case of arbitrarily strong pump waves.

A qualitative understanding of the origin of the predicted effects may be obtained by considering Fig. 1, which shows the energy levels $|a>$ and $|b>$ of an idealized two-level atom, separated by the atomic resonance frequency ω_{ba}. When a weak pump laser with frequency ω_1 is tuned near the atomic resonance, at a detuning of $\Delta=\omega_1-\omega_{ba}$, the laser creates two "virtual states," shown as broken lines in Fig. 1(a), one at an energy $\hbar\omega_1$ above the ground state $|a>$ and the other at an energy $\hbar\omega_1$ below the excited state $|b>$. It is known from theoretical[10] and experimental[11] work that photons from the laser will be scattered inelastically at the two frequencies $\omega_1+\Delta$, and ω_{ba}, as shown in Fig. 1(a) by wavy arrows. Scattering of a photon at frequency $\omega_1+\Delta$ is accompanied by the absorption of two laser photons; this process leaves the atom

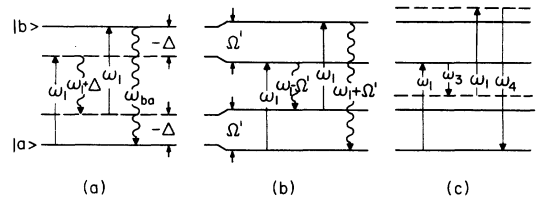

FIG. 1. (a) In the presence of a weak optical field at frequency ω_1, the two-level atom scatters light at the frequencies $\omega_1+\Delta$ and ω_{ba}. (b) In the presence of a strong optical field, each energy level splits into a doublet with separation Ω', and the atom then scatters light at the frequencies $\omega_1\pm\Omega'$. (c) A resonantly enhanced, parametric coupling can thus occur between the strong field at frequency ω_1 and two additional fields at frequencies ω_3 and ω_4, where $\omega_3+\omega_4=2\omega_1$.

in the excited state $|b>$, from which it may spontaneously emit a photon at the atomic frequency ω_{ba}. Since the ground state $|a>$ is more populated than the excited state $|b>$, the scattering at $\omega_1+\Delta$ can show gain, while any photons present at ω_{ba} will show loss due to absorption. The gain process at frequency $\omega_1+\Delta$ is often referred to as the "three-photon effect."

At large laser intensities the atomic energy levels will be shifted in energy by the ac Stark effect.[10] This shift becomes appreciable when the Rabi frequency $\Omega=|2\mu_{ba}E_1|/\hbar$ (where μ_{ba} is the atomic dipole matrix element and $2E_1$ is the amplitude of the laser's electric field) is comparable to the detuning Δ. In this situation it is convenient to use the language of dressed states,[12] which are the eigenstates of the atom-plus-laser-field system. Figure 1 (b) shows two pairs of the infinite ladder of possible dressed states. The pairs are separated by the energy $\hbar\omega_1$ of one laser photon, while the members of each pair are separated by an energy $\hbar\Omega'$, where

$$\Omega'=(\Delta^2+\Omega^2)^{1/2} \tag{1}$$

is the generalized Rabi frequency. As before, the system scatters photons inelastically, but now the scattered frequencies are $\omega_1+\Omega'$ and $\omega_1-\Omega'$, showing the effect of ac Stark shifting. These effects have been observed experimentally both in a collisionless[11] and a collisional[13] environment.

In this paper we point out that the effective four-level system of dressed states comprises a suitable medium for a *resonantly enhanced* four-wave mixing process, as shown in Fig. 1 (c). Consider, in addition to the strong pump laser wave at frequency ω_1, two weak probe waves at frequencies ω_3 and ω_4, where $\omega_3+\omega_4=2\omega_1$, and $\omega_3\simeq\omega_1-\Omega'$. In the absence of interaction between probe waves, the wave at ω_3 would experience gain by the three-photon effect, whereas the wave at ω_4 would experience loss by absorption. Under certain conditions, four-wave parametric coupling of the probe waves allows both waves to experience exponential growth. As the probe waves are tuned close to the resonance frequencies $\omega_1\pm\Omega'$ of the dressed-state system, an enhancement of the probe-wave gain is expected. This enhancement of the parametric gain by dressed-state energy levels is analagous to the enhancement by atomic or molecular energy levels in coherent anti-Stokes Raman scattering.

In Sec. II we review the theory of the nonlinear response of a single atom to a strong pump field at frequency ω_1 and a weak probe field at frequency ω_3. We display graphically the absorptive and dispersive responses at the probe frequency ω_3, and the response which can give rise to parametric coupling to a wave at frequency $2\omega_1-\omega_3$. In Sec. III we solve the spatial propagation equations for two probe waves coupled parametrically by the pump laser, and thereby determine the optimum conditions, including phase-matching conditions, for obtaining maximum gain. In Sec. IV we discuss the results and give an estimate of the gain under experimentally attainable conditions.

II. NONLINEAR RESPONSE OF A STRONGLY DRIVEN TWO-LEVEL SYSTEM

Let us consider an atom with ground state $|a>$ and excited state $|b>$, as in Fig. 1 (a), being driven by an arbitrarily intense pump electric field E_1 at frequency ω_1 and weak probe field E_3 at frequency ω_3, both tuned near the atomic resonance. Atomic motion will be ignored. The fields are denoted as

$$\vec{E}_i(\vec{r},t)=\hat{\epsilon}E_ie^{-i\omega_it}+\hat{\epsilon}^*E_i^*e^{i\omega_it}, \tag{2a}$$

where

$$E_i=A_ie^{i\vec{k}_i\cdot\vec{r}} \tag{2b}$$

for $i=1$ or 3. Here $\hat{\epsilon}$ is the polarization vector for the fields, and the $\vec{k}_i$ are the propagation vectors. These fields are assumed to be tuned near resonance, in the sense that the detunings are small compared to optical frequencies ($|\omega_i-\omega_{ba}|\ll\omega_{ba}$).

This problem was originally treated by Bloembergen and Shen[14] using density-matrix techniques and has subsequently been treated by other authors.[9,15,16] The results of these treatments are quoted here. The time evolution of the density-matrix elements ρ_{ij} is governed by the equations

$$\dot{\rho}_{ba}=-(i\omega_{ba}+1/T_2)\rho_{ba}+i\hbar^{-1}V_{ba}(\rho_{bb}-\rho_{aa}), \tag{3a}$$

$$\dot{\rho}_{ab}=\dot{\rho}_{ba}^*, \tag{3b}$$

$$\dot{\rho}_{bb}-\dot{\rho}_{aa}=(-1/T_1)[\rho_{bb}-\rho_{aa}-(\rho_{bb}-\rho_{aa})^0]+2i\hbar^{-1}(V_{ab}\rho_{ba}-\rho_{ab}V_{ba}), \tag{3c}$$

where T_1 and T_2 are the longitudinal and transverse relaxation times, respectively; $(\rho_{bb}-\rho_{aa})^0$ is the equilibrium population inversion in the absence of the optical fields; and V_{ba} is the interaction energy in the rotating-wave approximation

$$V_{ba}=V_{ab}^{*}=-\mu_{ba}(E_1e^{-i\omega_1 t}+E_3e^{-i\omega_3 t}),$$

with μ_{ba} being the dipole matrix element $\langle b|e\vec{r}|a\rangle\cdot\hat{\epsilon}$. In steady state the off-diagonal density-matrix element ρ_{ba} exhibits harmonic oscillations at an infinite number of frequencies of the form $n\omega_1\pm m\omega_3$ where n and m are integers. If the strong field E_1 is treated correctly to all orders while the weak probe field E_3 is treated to only first order, then ρ_{ba} oscillates at three dominant frequencies: ω_1, ω_3, and $2\omega_1-\omega_3$. We thus express ρ_{ba} in steady state in terms of Fourier amplitudes, denoted by $\rho_{ba}(\omega_i)$, as

$$\rho_{ba}=\rho_{ba}(\omega_1)e^{-i\omega_1 t}+\rho_{ba}(\omega_3)e^{-i\omega_3 t}+\rho_{ba}(2\omega_1-\omega_3)e^{-i(2\omega_1-\omega_3)t}. \tag{4}$$

The Fourier amplitudes are given (to all orders in E_1 and first order in E_3) by[9,14,15]

$$\rho_{ba}(\omega_1)=\frac{\mu_{ba}E_1(\rho_{bb}-\rho_{aa})^{dc}}{\hbar(\omega_1-\omega_{ba}+i/T_2)}, \tag{5a}$$

$$\rho_{ba}(\omega_3)=\frac{\mu_{ba}E_3(\rho_{bb}-\rho_{aa})^{dc}}{\hbar D(\omega_3)}\left[\left(\omega_3-\omega_1+\frac{i}{T_1}\right)\left(\omega_3-2\omega_1+\omega_{ba}+\frac{i}{T_2}\right)-\frac{2|\mu_{ab}|^2|E_1|^2(\omega_3-\omega_1)}{\hbar^2(\omega_1-\omega_{ba}-i/T_2)}\right], \tag{5b}$$

$$\rho_{ba}(2\omega_1-\omega_3)=\frac{2\mu_{ba}|\mu_{ab}|^2E_1^2E_3^{*}(\rho_{bb}-\rho_{aa})^{dc}(\omega_3-\omega_1+2i/T_2)}{\hbar^3D(\omega_3)(\omega_1-\omega_{ba}-i/T_2)} \tag{5c}$$

where $(\rho_{bb}-\rho_{aa})^{dc}$ is the steady-state saturated population inversion induced by the strong field E_1

$$(\rho_{bb}-\rho_{aa})^{dc}=\frac{[1+(\omega_1-\omega_{ba})^2T_2^2](\rho_{bb}-\rho_{aa})^0}{1+(\omega_1-\omega_{ba})^2T_2^2+4\hbar^{-2}|\mu_{ab}|^2|E_1|^2T_1T_2}, \tag{6}$$

and where $D(\omega_3)$ is the cubic function

$$D(\omega_3)=(\omega_3-\omega_1+i/T_1)(\omega_3-\omega_{ba}+i/T_2)(\omega_3-2\omega_1+\omega_{ba}+i/T_2)-4\hbar^{-2}|\mu_{ab}|^2|E_1|^2(\omega_3-\omega_1+i/T_2). \tag{7}$$

The physical consequences of the three terms in ρ_{ba} in Eq. (4) are as follows: $\rho_{ba}(\omega_1)$ and $\rho_{ba}(\omega_3)$ give rise to absorption (or amplification) of the pump and probe waves, respectively. Our main interest is in the consequences of the third term $\rho_{ba}(2\omega_1-\omega_3)$, which we shall call the "mixing response," because it gives rise to generation of an optical wave with frequency $\omega_4\equiv 2\omega_1-\omega_3$. If a wave at ω_4 is already present, it may be amplified by the effect of this term.

Before continuing with the full development of the problem, which requires the treatment of spatial propagation, and therefore the cumulative effect of many atoms, it is important to understand the behavior of the single-atom response, as given by Eqs. (4)–(7). To help gain insight into these rather complicated expressions, we have graphically displayed them for a wide range of the important parameters. In Figs. 2 and 3 we have graphed the imaginary and real parts of $\rho_{ba}(\omega_3)$ as a function of the detuning $(\omega_3-\omega_1)$ of the probe wave from the pump wave, in the case that the pump wave is tuned directly to the atomic resonance $(\omega_1=\omega_{ba})$ and the atomic line is broadened purely radiatively $(T_2/T_1=2)$. Figure 2 shows the behavior of the probe-wave absorption profile as the pump field strength (in terms of the Rabi frequency Ω) is increased from zero to well above saturation. The absorption profile first begins to saturate and then, at $\Omega T_2=2$, breaks up into a

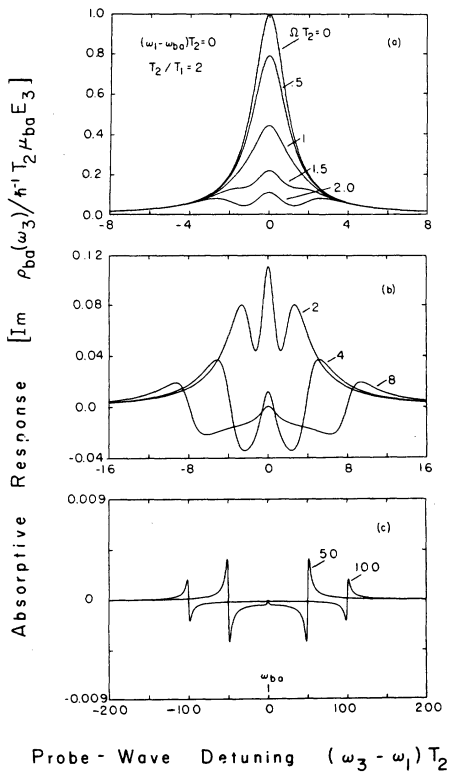

FIG. 2. The absorptive response is shown as a function of the probe-wave detuning for a pump wave detuning given by $(\omega_1-\omega_{ba})T_2=0$; and the case $T_2/T_1=2$, corresponding to purely radiative damping.

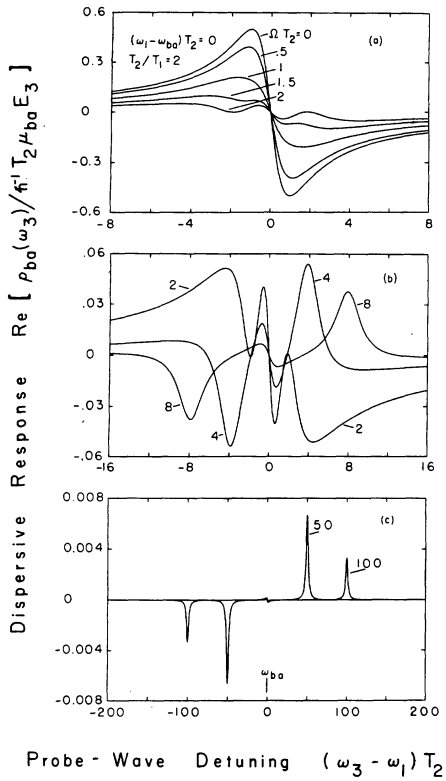

FIG. 3. The dispersive response is shown as a function of the probe-wave detuning for a pump wave detuning given by $(\omega_1-\omega_{ba})T_2=0$; and the case $T_2/T_1=2$, corresponding to purely radiative damping.

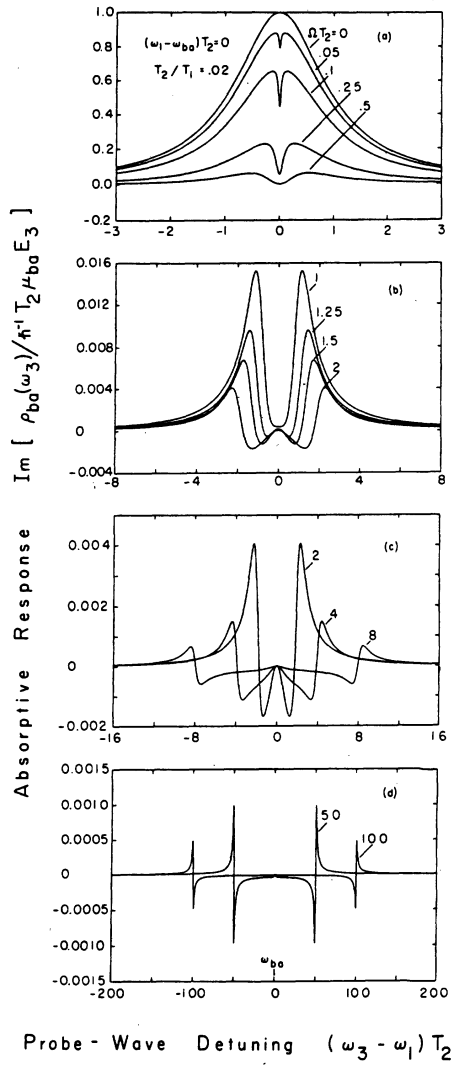

FIG. 4. The absorptive response is shown for a pump wave detuning given by $(\omega_1-\omega_{ba})T_2=0$; and the case $T_2/T_1=0.02$, corresponding to rapid collisional dephasing.

three-peaked spectrum, reminiscent of that in two-level-atom resonance fluorescence.[11] The positions of these peaks correspond to the three absorption frequencies between the two pairs of dressed states in Fig. 1 (b). As the pump field strength increases further, broad regions of gain appear between the absorption peaks. This type of behavior has been observed in an atomic beam.[17]

Figure 3 shows the corresponding behavior of the probe wave dispersion profile. The magnitude of the dispersion first decreases as the pump field strength is raised above saturation, and then the profile breaks up and finally, for very high fields, develops resonances at a detuning equal to the Rabi frequency. It is interesting, and perhaps surprising, that in the limit of large Rabi frequency [Fig. 3 (c)] the dispersion profile resembles two separated absorption profiles, while the absorption profile [Fig. 2 (c)] resembles two separated dispersion profiles.

In Figs. 4 and 5 we have illustrated the effects of rapid collisional dephasing on the absorption and dispersion profiles by taking the value $T_2/T_1=0.02$, again for the case of zero pump detuning $(\omega_1=\omega_{ba})$. For low Rabi frequencies the behavior is seen to be qualitatively different from the previous case of pure radiative damping. These curves decrease as a function of the parameter ΩT_2 faster than those for the pure radiative case of Figs. 2 and 3, since the parameter $\Omega\sqrt{T_1T_2}$ determines the amount of saturation. In addition to a general decrease in the magnitude of the absorption profile in Fig. 4 (a) as the pump field is increased, a narrow hole is "burned" into the homogeneously broadened probe-wave absorption profile.[16] As the Rabi frequency is increased from zero to a large value [Figs. 4 (d) and 5 (d)] the absorption and dispersion profiles again exchange shapes.

The origin of the "hole burning" dip in Fig. 4 (a) is in the so-called "coherent population oscilla-

tions"[18] which are induced by the pump and probe waves beating together at the difference frequency $\omega_3-\omega_1$. A simple analytical expression can be derived for the shape of the dip as follows. When the dephasing width T_2^{-1} is large compared to the Rabi frequency and the beat frequency ($T_2^{-1}\gg\Omega$, $|\omega_3-\omega_1|$), Eq. 3(a) can be solved approximately to give the steady-state result

$$\rho_{ba}(t)\simeq-\frac{i\mu_{ba}}{\hbar}\frac{E_1e^{-i\omega_1t}+E_3e^{-i\omega_3t}}{i(\omega_{ba}-\omega_1)+1/T_2}[\rho_{bb}(t)-\rho_{aa}(t)]\,. \quad (8)$$

This shows the familiar fact that the polarization in the medium is proportional to the product of the driving field strength and the population inversion. When this result for $\rho_{ba}(t)$ is used in Eq. (3c), a rate equation is obtained for the population inversion:

$$\dot\rho_{bb}-\dot\rho_{aa}=(-1/T_1)[\rho_{bb}-\rho_{aa}-(\rho_{bb}-\rho_{aa})^0]-\frac{4T_2|\mu_{ba}|^2}{\hbar^2[1+(\omega_1-\omega_{ba})^2T_2^2]}(E_1^2+E_3^2+2E_1E_3\cos\delta t)(\rho_{bb}-\rho_{aa})\,, \quad (9)$$

where $\delta=\omega_3-\omega_1$ is the probe-wave detuning and where, for simplicity, we have taken E_1 and E_3 to be real. Assuming also that $(\rho_{bb}-\rho_{aa})^0=-1$, the rate equation (9) can be solved in steady state to give

$$\rho_{bb}-\rho_{aa}=\frac{-1}{T_1}\int_{-\infty}^{t}e^{-\beta(t-t')}e^{-(\gamma/\delta)(\sin\delta t-\sin\delta t')}dt'\,, \quad (10)$$

where

$$\beta=\frac{1}{T_1}+\frac{4T_2|\mu_{ba}|^2}{\hbar^2[1+(\omega_1-\omega_{ba})^2T_2^2]}(E_1^2+E_3^2) \quad (11a)$$

and

$$\gamma=\frac{4T_2|\mu_{ba}|^2}{\hbar^2[1+(\omega_1-\omega_{ba})^2T_2^2]}(2E_1E_3)\,. \quad (11b)$$

The parameter β may be interpreted as the rate of population-inversion decay induced by both spontaneous emission and laser pumping. In the case of interest here, the probe wave is much weaker than the pump wave ($E_3\ll E_1$) and therefore $\gamma\ll\beta$, which allows Eq. (10) to be evaluated as

$$\rho_{bb}-\rho_{aa}\simeq(\rho_{bb}-\rho_{aa})^{dc}+(\rho_{bb}-\rho_{aa})^{(\delta)}e^{i\delta t}+(\rho_{bb}-\rho_{aa})^{(-\delta)}e^{-i\delta t}\,, \quad (12)$$

where $(\rho_{bb}-\rho_{aa})^{dc}$ is the dc component of the population inversion given in Eq. (6) and $(\rho_{bb}-\rho_{aa})^{(\pm\delta)}$ are the amplitudes of the components oscillating at the beat frequency δ, and are given by (see Appendix)

$$(\rho_{bb}-\rho_{aa})^{(\pm\delta)}=\frac{\gamma}{2T_1}\frac{1\mp i\delta/\beta}{\delta^2+\beta^2}\,. \quad (13)$$

From Eq. (13) we see that coherent population oscillations are significant when $\delta\lesssim\beta$, that is, when the beat frequency δ is less than the rate of population-inversion decay.

To see how this oscillating population affects the absorption of the probe wave E_3, we substitute Eq. (12) into Eq. (8) and collect those terms in the off-diagonal density-matrix element $\rho_{ba}(t)$ which oscillate at the probe-wave frequency ω_3. This gives for the Fourier amplitude

$$\rho_{ba}(\omega_3)=-\frac{i\mu_{ba}}{\hbar}\frac{1}{i(\omega_{ba}-\omega_1)+1/T_2}\times[E_3(\rho_{bb}-\rho_{aa})^{dc}+E_1(\rho_{bb}-\rho_{aa})^{(-\delta)}]\,. \quad (14)$$

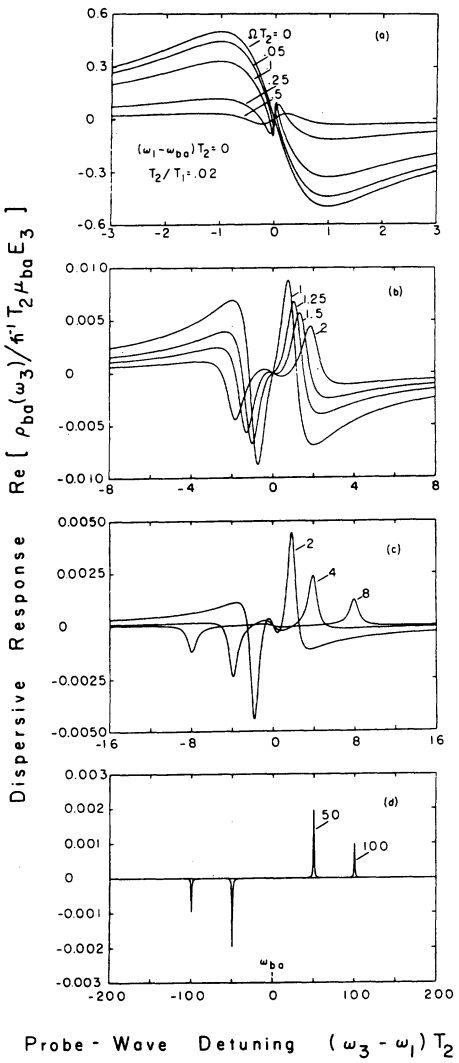

FIG. 5. The dispersive response is shown for a pump wave detuning given by $(\omega_1-\omega_{ba})T_2=0$; and the case $T_2/T_1=0.02$, corresponding to rapid collisional dephasing.

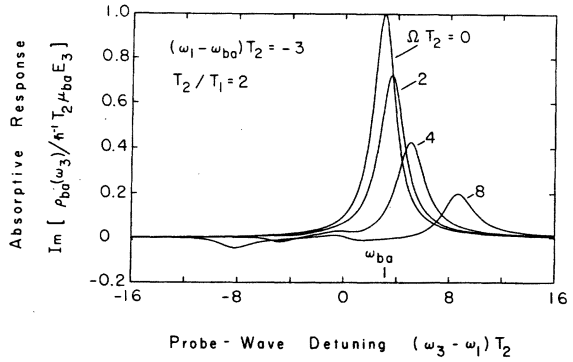

FIG. 6. The absorptive response is shown for a pump-wave detuning given by $(\omega_1-\omega_{ba})T_2=-3$ and the case $T_2/T_1=2$.

We see that the component of the dipole moment oscillating at frequency ω_3 is composed of two parts: the part proportional to E_3 is driven directly by the E_3 wave, while the part proportional to E_1 results from the population oscillations at frequency δ beating against the pump wave at frequency ω_1. The shape of the dip in the probe-wave absorption profiles in Fig. 4(a) may be obtained by finding the imaginary part of $\rho_{ba}(\omega_3)$ in Eq. (14) with $\omega_1=\omega_{ba}$, to give

$$\mathrm{Im}\rho_{ba}(\omega_3)=\frac{\mu_{ba}E_3T_2}{\hbar}\left(-(\rho_{bb}-\rho_{aa})^{dc}-\frac{\Omega^2T_2}{T_1}\frac{1}{\delta^2+\beta^2}\right), \tag{15}$$

In this case β, which is now seen to be the half width of the dip, is given by

$$\beta=(1/T_1)(1+\Omega^2T_1T_2), \tag{16}$$

showing the effects of power broadening when $\Omega^2T_1T_2\gtrsim 1$. The simple formula in Eq. (15) predicts accurately the depth and width of the four dips in Fig. 4(a).

In Figs. 6–9 we have displayed the absorptive and dispersive responses for the case that the

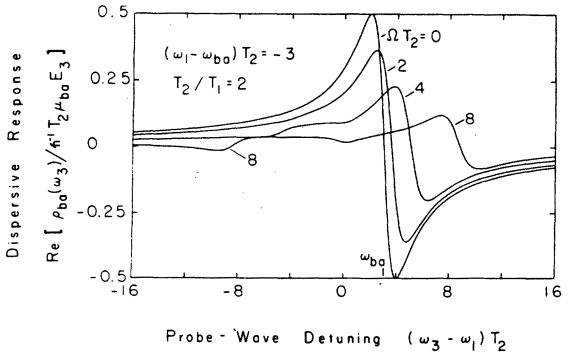

FIG. 7. The dispersive response is shown for a pump wave detuning given by $(\omega_1-\omega_{ba})T_2=-3$ and the case $T_2/T_1=2$.

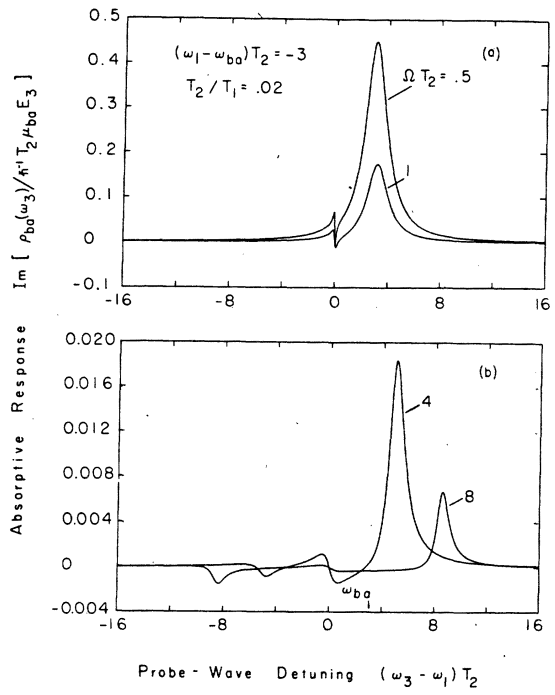

FIG. 8. The absorptive response for a pump-wave detuning given by $(\omega_1-\omega_{ba})T_2=-3$ and the case $T_2/T_1=0.02$.

pump laser is detuned from the atomic resonance by three line widths, $\omega_1-\omega_{ba}=-3T_2^{-1}$. Figure 6 shows the responses for the case of pure radiative

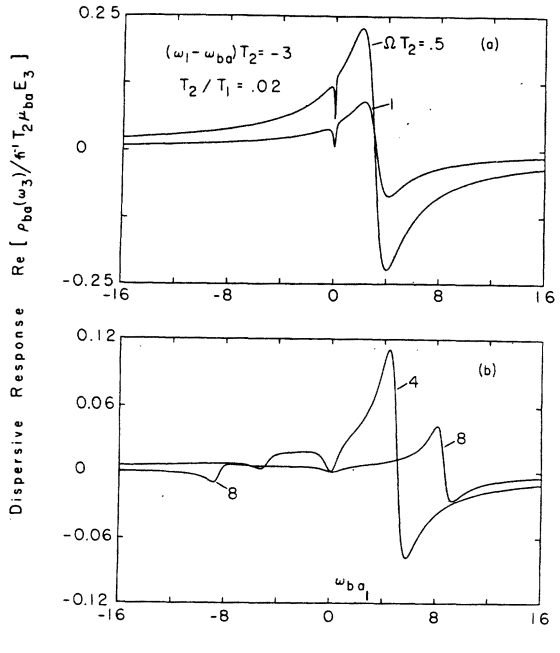

FIG. 9. The dispersive response for a pump-wave deturning given by $(\omega_1-\omega_{ba})T_2=-3$ and the case $T_2/T_1=0.02$.

damping, corresponding to $T_2/T_1=2$. As the pump Rabi frequency increases, the absorption profile in Fig. 6 saturates, and positive and negative absorption peaks appear at frequencies symmetrically displaced from the pump frequency by the generalized Rabi frequency Ω', again as expected from the discussion of the three-photon effect in Fig. 1. Figure 7 shows the complementary behavior of the dispersion profile. Figures 8 and 9 show the absorptive and dispersive responses for the case of rapid dephasing, corresponding to $T_2/T_1=0.02$. Figure 8(a) shows the behavior of the hole burning in the homogeneous profile when the pump laser is detuned from the atomic resonance. The dip in the probe absorption profile, which again is caused by the coherent population oscillations, is seen to occur at the position of the pump laser frequency. The positions and shapes of the dips in Fig. 8(a) are properly accounted for by Eq. (15). When $\Omega T_2=8$, in Fig. 8(b), the absorption profile is seen to be qualitatively similar to that in Fig. 6 for purely radiative damping. The dispersion profiles corresponding to the absorption profiles in Fig. 8 are shown in Fig. 9. Again, complementary behavior between dispersive-looking and absorptive-looking features, as required by the Kramers-Kronig relations, is evident.

In Fig. 10 we have graphed the absolute value of the mixing response $|\rho_{ba}(2\omega_1-\omega_3)|$ which, as mentioned above, gives rise to generation or amplification of a wave at frequency $\omega_4\equiv 2\omega_1-\omega_3$. This term provides the coupling for four-wave parametric mixing, which will be discussed in detail in the following section. Figure 10(a), which is plotted for pure radiative damping ($T_2/T_1=2$), shows that for zero pump detuning ($\omega_1=\omega_{ba}$) and at small pump fields ($\Omega T_2=0.4$) the mixing response is maximum when the probe frequency ω_3 is very close to the pump frequency ω_1. The peak of this resonance corresponds to degenerate four-wave mixing. At high pump Rabi frequencies, however, the profile breaks up into a three-peaked spectrum, with peaks displaced from the pump frequency by the generalized Rabi frequency Ω'. This result is as expected from the simple discussion of the dressed states in Fig. 1(c), and is the basis for the qualitatively new effects predicted in this paper. Figure 10(b) illustrates the effects of rapid collisional dephasing ($T_2/T_1=0.02$) on the zero-detuning ($\omega_1=\omega_{ba}$) profile. It is seen that again at small fields ($\Omega T_2=0.01$, 0.03) the mixing response shows a resonance at the pump frequency ($\omega_3=\omega_1$). The origin of this narrow resonance, whose half-width is T_1^{-1}, is the same coherent population oscillations which gave rise to the dip in the probe-wave absorption profile in Fig. 4(a). By substituting Eq. (12) into Eq. (8), and this time collecting

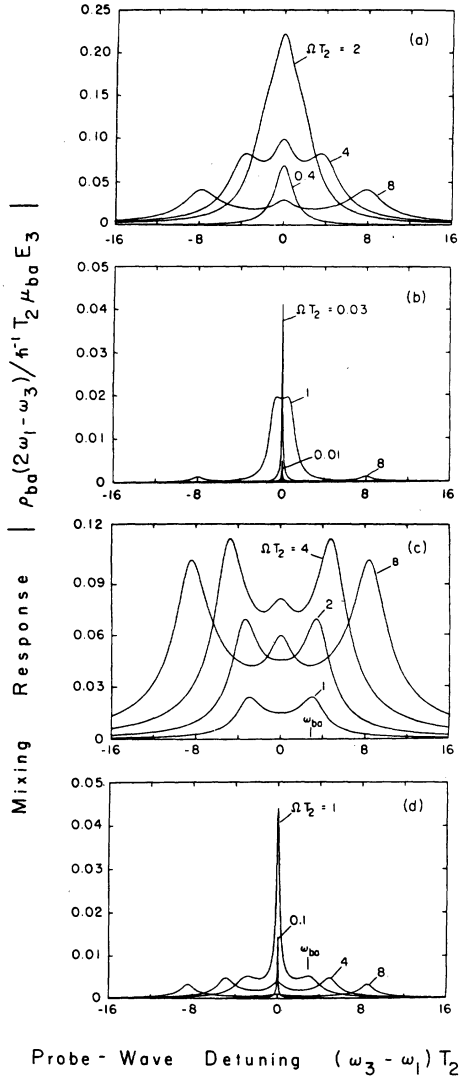

FIG. 10. The modulus of the mixing response is shown as a function of the probe-wave detuning for the following cases: (a) $(\omega_1-\omega_{ba})T_2=0$, $T_2/T_1=2$; (b) $(\omega_1-\omega_{ba})T_2=0$, $T_2/T_1=0.02$; (c) $(\omega_1-\omega_{ba})T_2=-3$, $T_2/T_1=2$; (d) $(\omega_1-\omega_{ba})T_2=-3$, $T_2/T_1=0.02$.

terms which oscillate at the frequency $2\omega_1-\omega_3=\omega_1-\delta$, the Fourier amplitude $\rho_{ba}(2\omega_1-\omega_3)$ can be found, yielding

$$|\rho_{ba}(2\omega_1-\omega_3)|=\frac{\mu_{ba}E_3\Omega^2T_2^2}{\hbar\beta T_1[1+(\omega_1-\omega_{ba})^2T_2^2]^{1/2}}-\frac{1}{(\delta^2+\beta^2)^{1/2}}. \tag{17}$$

This simple expression accounts for the height and width of the narrow resonances seen for $\Omega T_2=0.01$, 0.03. At higher Rabi frequency ($\Omega T_2=8$) the mixing profile again breaks up into peaks at the generalized Rabi frequency.

Figures 10(c) and 10(d) show the mixing re-

sponse obtained when the pump laser is detuned from resonance by three line widths, $\omega_1 - \omega_{ba} = -3T_2^{-1}$. While Fig. 10(d) shows a narrow resonance again appearing at the pump laser frequency ω_1 when rapid collisions are present, Fig. 10(c) shows no such resonance in the absence of collisions. It is notable that in all four plots the resonances occurring at the generalized Rabi frequency Ω' are the dominant features in the case of high laser intensity ($\Omega T_2 = 8$).

III. SPATIAL PROPAGATION AND PARAMETRIC GAIN

In this section we study spatial propagation effects by using the nonlinear polarization, which is proportional to the off-diagonal elements of the density matrix, as a source term in the Helmholtz wave equation. This treatment will show that four-wave parametric amplification is achievable under certain conditions. The three interacting fields are defined as before by Eq. (2), where now $i = 1$, 3, or 4. We assume that the pump wave at ω_1 is not depleted by its interaction with the atomic system and we thus take its amplitude A_1 to be constant. The probe-field amplitudes $A_3(\vec{r})$ and $A_4(\vec{r})$ are not constant, however, since they are coupled by a nonlinear polarization of the form

$$\vec{P}_i(\vec{r}, t) = \hat{\epsilon} P_i e^{-i\omega_i t} + \hat{\epsilon}^* P_i^* e^{i\omega_i t} . \tag{18}$$

The amplitudes P_i of the polarization are proportional to the off-diagonal density-matrix elements calculated in the previous section. The form of the coupling between the weak fields is clearly displayed if the polarization amplitudes are expressed in terms of the susceptibility as

$$P_3 = \chi^{(1)}(\omega_3, |E_1|)E_3 + \chi^{(3)}(\omega_3 = 2\omega_1 - \omega_4, |E_1|)E_1^2 E_4^* , \tag{19a}$$

$$P_4 = \chi^{(1)}(\omega_4, |E_1|)E_4 + \chi^{(3)}(\omega_4 = 2\omega_1 - \omega_3, |E_1|)E_1^2 E_3^* , \tag{19b}$$

where the elements of the susceptibility are related to the elements of the density matrix [given in Eq. (5)] by

$$\chi^{(1)}(\omega_3, |E_1|) = -N\mu_{ab}\rho_{ba}(\omega_3)/E_3 , \tag{20a}$$

$$\chi^{(1)}(\omega_4, |E_1|) = -N\mu_{ab}\rho_{ba}(\omega_4)/E_4 , \tag{20b}$$

$$\chi^{(3)}(\omega_3 = 2\omega_1 - \omega_4, |E_1|) = -N\mu_{ab}\rho_{ba}(\omega_3 = 2\omega_1 - \omega_4)/E_1^2 E_4^* , \tag{20c}$$

$$\chi^{(3)}(\omega_4 = 2\omega_1 - \omega_3, |E_1|) = -N\mu_{ab}\rho_{ba}(\omega_4 = 2\omega_1 - \omega_3)/E_1^2 E_3^* , \tag{20d}$$

where N is the number density of atoms. Defined in this manner, the elements of the nonlinear susceptibility are independent of position and of the weak-field amplitudes, but do depend on the pump-field amplitude $|E_1|$. This nonlinear susceptibility is thus a generalization of the usual susceptibility in that it properly accounts for atomic saturation. Since the real part of $\chi^{(1)}(\omega_i, |E_1|)$ contributes to the refractive index for the wave at frequency ω_i, the Helmholtz equation for the wave at frequency ω_3 can be written in the form

$$\nabla^2 E_3 + k_3^2 E_3 = \frac{4\pi\omega_3^2}{c^2}[i\,\mathrm{Im}\chi^{(1)}(\omega_3, |E_1|)E_3 + \chi^{(3)}(\omega_3 = 2\omega_1 - \omega_4, |E_1|)E_1^2 E_4^*] \tag{21}$$

and the Helmholtz equation for the wave at ω_4 can be written in the same form under the interchange of the subscripts 3 and 4. Here the propagation constant k_i is given by

$$k_i = n_i\omega_i/c$$

with

$$n_i = n_0 + 2\pi\,\mathrm{Re}\chi^{(1)}(\omega_i, |E_1|) ,$$

n_0 denoting the refractive index of the vacuum, or of any buffer gas present. It is convenient to define the propagation direction of the pump wave to be the positive z direction, which is taken to be perpendicular to the input face of the nonlinear medium, and to consider the three waves to be nearly copropagating in the sense that the sine of the angle between the propagation directions of any two of the three interacting waves is much less than unity. By further introducing the slowly varying envelope, or adiabatic, approximation

$$\left|\frac{\partial^2 A_i}{\partial z^2}\right| \ll k_i \left|\frac{\partial A_i}{\partial z}\right| , \quad i = 3, 4 ,$$

the Helmholtz equations become

$$\frac{\partial A_3}{\partial z} = -\alpha_3 A_3 + \kappa_3 A_4^* e^{i\Delta kz} , \tag{22a}$$

$$\frac{\partial A_4^*}{\partial z} = -\alpha_4 A_4^* + \kappa_4^* A_3 e^{-i\Delta kz} , \tag{22b}$$

where Δk is the z component of the propagation vector mismatch

$$\overrightarrow{\Delta k} = 2\vec{k}_1 - \vec{k}_3 - \vec{k}_4 , \tag{23}$$

which is constrained by phase-matching considerations to be perpendicular to the input face, as shown in Fig. 11, and where the coupling constants are defined by

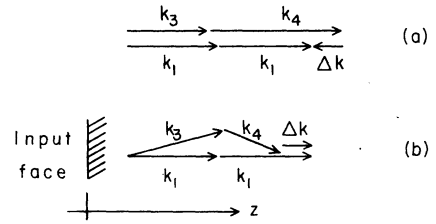

FIG. 11. The phase matching conditions are shown for (a) colinear and (b) noncolinear propagation. Note that the scalar mismatch $\Delta k = \overrightarrow{\Delta k} \cdot \hat{z}$ is greater in (b) than in (a).

$$\alpha_3 = -2\pi \frac{\omega_3}{n_3 c} \mathrm{Im}\chi^{(1)}(\omega_3, |E_1|), \tag{24a}$$

$$\alpha_4 = -2\pi \frac{\omega_4}{n_4 c} \mathrm{Im}\chi^{(1)}(\omega_4, |E_1|), \tag{24b}$$

$$\kappa_3 = -2\pi i \frac{\omega_3}{n_3 c} \chi^{(3)}(\omega_3 = 2\omega_1 - \omega_4, |E_1|) A_1^2, \tag{24c}$$

$$\kappa_4 = -2\pi i \frac{\omega_4}{n_4 c} \chi^{(3)}(\omega_4 = 2\omega_1 - \omega_3, |E_1|) A_1^2. \tag{24d}$$

The coupled amplitude Eqs. (22) can be solved for arbitrary initial values A_3^0 and A_4^0 of the field amplitudes $A_3(z)$ and $A_4(z)$ at the boundary $z=0$ of the nonlinear medium to give

$$A_3(z) = (g_+ - g_-)^{-1}\{[\kappa_3 A_4^{0*} - (g_- + \alpha_3 + i\Delta k/2)A_3^0]e^{g_+ z} - [\kappa_3 A_4^{0*} - (g_+ + \alpha_3 + i\Delta k/2)A_3^0]e^{g_- z}\} \times e^{i\Delta k z/2}, \tag{25a}$$

$$A_4^*(z) = (g_+ - g_-)^{-1}\{[\kappa_4^* A_3^0 - (g_- + \alpha_4 - i\Delta k/2)A_4^{0*}]e^{g_+ z} - [\kappa_4^* A_3^0 - (g_+ + \alpha_4 - i\Delta k/2)A_4^{0*}]e^{g_- z}\} \times e^{-i\Delta k z/2}, \tag{25b}$$

where the gain coefficients $g_\pm$ are given by

$$g_\pm = \pm\tfrac{1}{2}[(\alpha_3 - \alpha_4 + i\Delta k)^2 + 4\kappa_3\kappa_4^*]^{1/2} - \tfrac{1}{2}(\alpha_3 + \alpha_4). \tag{26}$$

The amplitudes A_3 and A_4^* thus consist of linear combinations of two solutions with exponential z dependence. From the definition of $g_\pm$ it is seen that the real part of g_+ is always greater than the real part of g_-. Under appropriate circumstances the real part of g_+ can be positive and the medium will thus show gain. The amplitudes A_3 and A_4^* are also functions of the phase mismatch per unit length Δk.

While Eqs. (25) and (26) constitute a complete solution to the propagation problem, their form is rather complicated, and thus some intuition into their nature is afforded by considering the case where all three waves are detuned many linebreadths T_2^{-1} from the line center and where the pump intensity $|A_1|^2$ is sufficiently small that only the lowest-order contributions to the nonlinear susceptibilities in Eq. (20) need be considered. Furthermore, the absorption coefficients α_3 and α_4 are then negligible compared to the mixing coefficients κ_3 and κ_4 as long as the pump intensity is not too small, and in this case the gain coefficients take the simple form

$$g_\pm = \pm\tfrac{1}{2}(4\kappa_3\kappa_4^* - \Delta k^2)^{1/2}, \tag{27}$$

where κ_3 and κ_4 are given by Eqs. (24c) and (24d), and where the susceptibilities are now real quantities and are given by the expression

$$\chi^{(3)}(\omega_3 = 2\omega_1 - \omega_4, |E_1|) = \chi^{(3)}(\omega_4 = 2\omega_1 - \omega_3, |E_1|) = \frac{2\hbar^{-3} N |\mu_{ba}|^4}{(\omega_1 - \omega_{ba})(\omega_3 - \omega_{ba})(\omega_4 - \omega_{ba})}. \tag{28}$$

This form for the susceptibility can be derived using third-order, time-dependent perturbation theory, and is the form used in an earlier treatment[7] of four-wave mixing with two counter-propagating pump waves. Since $\kappa_3 = \kappa_4$ for this choice of the susceptibilities, the product $\kappa_3\kappa_4^*$ is real, and thus the gain coefficient obtains its maximum real value $g_+ = -g_- = |\kappa_3| = |\kappa_4|$ for $\Delta k = 0$. For this case of perfect phase matching $\Delta k = 0$, the wave amplitudes $A_3(z)$ and $A_4^*(z)$ of Eqs. (25) are given by the simple expression

$$A_3(z) = \tfrac{1}{2}A_3^0(e^{g_+ z} + e^{g_- z}) \mp \tfrac{1}{2}iA_4^{0*}(e^{g_+ z} - e^{g_- z}), \tag{29a}$$

$$A_4^*(z) = \tfrac{1}{2}A_4^{0*}(e^{g_+ z} + e^{g_- z}) \pm \tfrac{1}{2}iA_3^0(e^{g_+ z} - e^{g_- z}), \tag{29b}$$

where the upper or lower sign is to be taken depending on whether $\chi^{(3)}(\omega_4 = 2\omega_1 - \omega_3, |E_1|)$ has a positive or negative value, respectively. It can be shown analytically that the choice $\Delta k = 0$ maximizes the intensities of both output waves for arbitrary initial conditions, as long as there is no temporal coherence between the input waves. The solutions (29) show that an incident wave at either frequency ω_3 or ω_4 can create and/or amplify waves at both frequencies ω_3 and ω_4. The two waves grow purely as a result of their parametric coupling via four-wave mixing, in contrast to the more general case where the three-photon effect [Fig. 1(b)] constitutes a mechanism for nonparametric gain.

The solutions given in equations (29) are for $\Delta k = 0$. If all three waves are tuned to the low-frequency side of resonance, the phase mismatch Δk will be negative for colinear propagation and thus the optimum phase-matching condition $\Delta k = 0$ can be achieved for some relative orientation of the probe beams. Conversely, if the waves are tuned to the high frequency side, perfect phase matching $\Delta k = 0$ will not be possible.

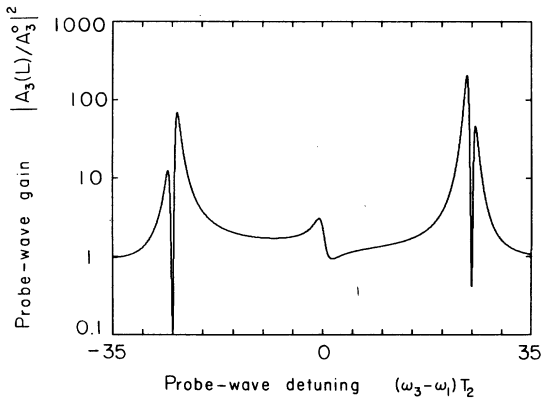

FIG. 12. The probe-wave gain is shown as a function of the probe wave detuning for the case $(\omega_1-\omega_{ba})T_2=8$; $\Omega' T_2=25$, $T_2/T_1=0.02$, $\alpha_0 L=2500$, and $\Delta k=0$.

For the more general case in which we cannot assume large detunings and weak fields, the general form of the wave equation solution (25), (26) must be used, and for this case we again take the approach of graphically displaying the solutions for some typical cases. In Fig. 12 the probe-wave gain $|A_3(L)/A_3^0|^2$ is plotted as a function of $\omega_3-\omega_1$ under the assumption of equal input amplitudes $A_3^0=A_4^0$, and using the conditions $T_2/T_1=0.02$, corresponding to a collision-dominated medium; $(\omega_1-\omega_{ba})T_2=8$; $\Omega' T_2=25$; $\Delta k=0$, corresponding to the condition of perfect phase matching; and $\alpha_0 L=2500$, L being the length of the medium and α_0 being the weak-field, line center, absorption coefficient given by

$$\alpha_0=4\pi N\omega_{ba}|\mu_{ab}|^2 T_2/\hbar c\,. \tag{30}$$

The form of the gain curve illustrates resonant enhancement for probe fields detuned from the pump field by approximately the generalized Rabi frequency Ω'.

In order to illustrate the origin of the dips in the gain curve exactly at the generalized Rabi frequency, we have plotted in Fig. 13 the output intensity of the waves at frequencies $\omega_3=\omega_1\pm\Omega'$ as a function of the phase mismatch Δk. These curves show a sharp decrease in output power at perfect phase matching, $\Delta k=0$. This occurs because the wave at $\omega_1+\Omega'$ shows gain by the three-photon effect, while the other wave at $\omega_1-\Omega'$ shows loss by absorption. Thus, the wave at $\omega_1+\Omega'$ is suppressed by strong coupling ($\Delta k=0$) to the one at $\omega_1-\Omega'$, and shows maximum gain for increasingly weak coupling (Δk large), while the wave at $\omega_1-\Omega'$ shows maximum gain when the coupling is strong enough to allow it to be dragged along by the wave at $\omega_1+\Omega'$, but not strong enough to prevent the growth of *both* waves. This effect is

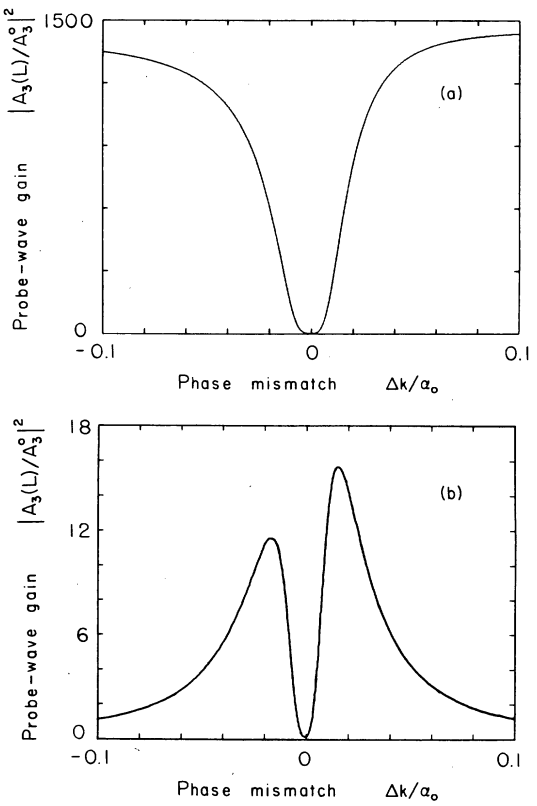

FIG. 13. The probe-wave gain is shown as a function of the phase mismatch at the frequencies: (a) $\omega_3=\omega_1+\Omega'$ and (b) $\omega_3=\omega_1-\Omega'$ for the same choice of parameters used in Fig. 12.

analogous to the suppressed production of Stokes and anti-Stokes radiation in the phase-matched direction for the case of stimulated Raman scattering.[19]

To illustrate the behavior discussed above we show in Fig. 14(a) a gain curve obtained using the same parameters as in Fig. 12, except that instead of taking $\Delta k=0$ we have, at each value of ω_3, selected numerically that value of Δk, shown in Fig. 14(b), which maximizes the output intensity $|A_3(L)|^2$. In performing this optimization we have assumed that Δk can be varied only by changing the propagation directions of the probe beams, and thus Δk is constrained to be greater than or equal to the value of Δk obtained for colinear propagation, as shown in Fig. 11. For the peak at $\omega_3=\omega_1+\Omega'$, Fig. 14(b) shows that optimum generation requires a very large phase mismatch. This large mismatch has the effect of decoupling the probe waves, so that the wave at ω_3 grows almost entirely by the three-photon effect and the wave at $\omega_4=\omega_1-\Omega'$ thus shows no gain. For the peak at $\omega_3=\omega_1-\Omega'$, Fig. 14(b) shows that optimum generation requires a large but finite phase mis-

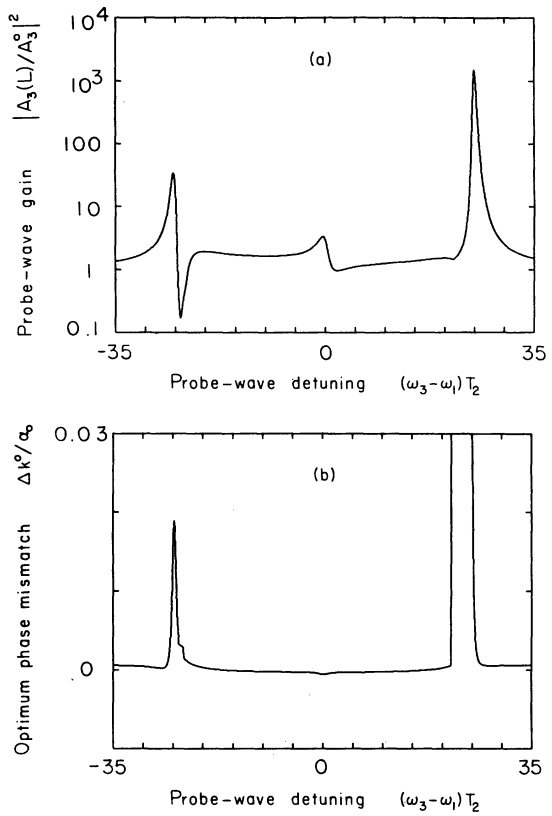

FIG. 14. (a) The probe-wave gain is shown for the same parameters as in Fig. 12, except that, at each value of ω_3, Δk is numerically selected to maximize the intensity of the output wave. (b) The resulting optimum phase mismatch $\Delta k^0/\alpha_0$ is shown.

match, which allows the waves to couple, but only weakly. The wave at $\omega_4 = \omega_1 + \Omega'$ can then grow by the three-photon effect, and the wave at ω_3 is dragged along by the parametric coupling and shows net gain.

In Fig. 15 we show the gain curve which is analogous to that of Fig. 14 but for the case $T_2/T_1 = 2$, indicating pure radiative damping, and $\alpha_0 L = 100$, chosen because of the larger gain for this case. The parameters $(\omega_1 - \omega_{ba})T_2 = 8$ and $\Omega' T_2 = 25$ are again used, and Δk is chosen to optimize the output intensity. In addition to the gain being larger in this case, the gain curve is broader in terms of the dimensionless frequency $(\omega_3 - \omega_1)T_2$.

The curves shown in Figs. 12–15 assume the boundary conditions $A_3^0 = A_4^0$, corresponding to equal input intensities. The results are found to be qualitatively similar if boundary conditions of the form $A_3^0 \neq 0$, $A_4^0 = 0$ are taken, which shows that an input at either ω_3 or ω_4 is sufficient to generate output waves at both ω_3 and ω_4.

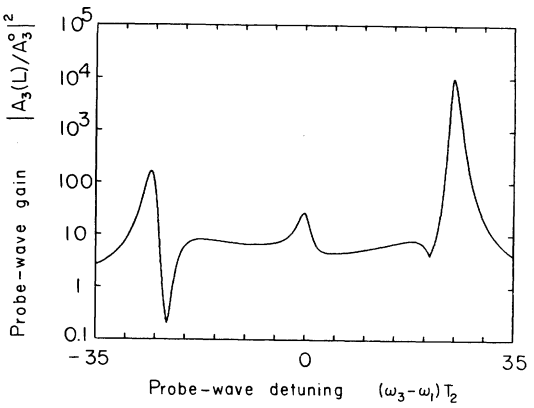

FIG. 15. The probe wave gain is shown for the case $(\omega_1 - \omega_{ba})T_2 = 8$, $\Omega' T_2 = 25$, $T_2/T_1 = 2$, $\alpha_0 L = 100$, and Δk selected, at each value of ω_3, to maximize the output intensity.

IV. DISCUSSION

The treatment of propagation effects given in the last section indicates that under certain conditions large gain is achievable by four-wave parametric amplification. We wish to point out here that these conditions may be met in typical experimental situations. Consider a vapor of atoms having a resonance transition with oscillator strength equal to unity, at a wavelength of 6000 Å. The two relevant levels will then be connected by a dipole transition moment with magnitude $\mu = 6.5 \times 10^{-18}$ esu, leading to a full width at half maximum (FWHM) natural line breadth $\Delta\nu = (2\pi T_1)^{-1} = 10$ MHz.

The theory presented in this paper does not treat transitions whose breadth is due predominately to inhomogeneous broadening. In an atomic vapor, Doppler broadening will lead typically to an inhomogeneous line breadth of 1 GHz. Collisions can increase the homogeneous line breadth well beyond the radiative breadth, however, and if the collisional line breadth is much greater than the Doppler line breadth, the theory presented here is expected to be valid. The case where the collisional line breadth $(\pi T_2)^{-1}$ is just equal to the Doppler breadth comprises a limiting case to the general applicability of this theory and corresponds to the condition $T_2/T_1 = 0.02$ used in many of our numerical examples. Collisional broadening may result from broadening by a foreign buffer gas or may result from self-broadening. The latter mechanism limits the number density of atoms of the active species that can be present, without exceeding the 1 GHz line breadth assumed above, to be less than 10^{16} cm^{-3}.

We shall consider for illustration the experi-

mental conditions for which the gain predicted by Fig. 14(a) would be measurable. Using the value $T_2 = 0.32$ nsec implicity assumed above, the parameters used to generate Fig. 14(a) correspond to a pump laser detuned 4.0 GHz to the blue side of line center, and the peaks in the gain curve occur at detunings of ±12 GHz from the laser frequency. All three waves are thus detuned from line center by many Doppler breadths, further reducing the effects of any residual inhomogeneous broadening. The number density of the active species is chosen as 5×10^{14} cm^{-3}, and the number density of the buffer gas is chosen to give a collisional line breadth of 1 GHz, and is thus approximately 10^{18} cm^{-3}. An interaction length of $L = 1.0$ cm therefore corresponds to the value $\alpha_0 L = 2500$ assumed in the figure. For the value of the matrix element μ assumed above, the Rabi frequency $\Omega = 2\pi$ (11.8 GHz) assumed in Fig. 14 requires a laser intensity of 17 kW/cm^2. Assuming the beam is focused such that its confocal parameter is equal to L, this intensity can be obtained with a laser power of 200 mW.

Tam[20] has recently reported the amplification of a weak probe wave, derived from his pump laser, in the presence of a cw laser beam focused into sodium vapor, and Skinner and Kleiber[21] have recently reported the generation of radiation at new frequencies, emitted in conical rings, by focussing a pulsed laser into barium vapor. We have verified experimentally that rings of the type observed by Skinner and Kleiber are also produced in sodium vapor, and we are attempting to explain their origin in terms of the four-wave parametric process described here. Other complicating effects, such as self-focusing, will have to be taken into account.

Finally, the large gain predicted by our calculation suggests that by enclosing the nonlinear medium in an optical cavity resonant at frequencies ω_3 or ω_4, or both, it should be possible to construct a four-wave parametric oscillator based on resonantly enhanced mixing near a two-level resonance. Such a device might be useful for converting the output of a fixed-frequency laser into radiation tunable over a modest spectral range.

ACKNOWLEDGMENTS

The authors wish to thank C. R. Stroud, Jr., and J. H. Eberly for useful discussions. This work was partially supported by the National Science Foundation, the Royal Norwegian Council for Scientific and Industrial Research, and the Norwegian Defence Research Establishment.

APPENDIX

In this Appendix we shall describe the approximation method which, under the provision $\gamma \ll \beta$, leads from Eq. (10) to Eqs. (12) and (13). Starting from Eq. (10), which is reproduced here

$$\rho_{bb} - \rho_{aa} = -\frac{1}{T_1}\int_{-\infty}^{t} e^{-\beta(t-t')} e^{-(\gamma/\delta)(\sin\delta t - \sin\delta t')} dt' , \tag{A1}$$

we consider two limiting cases, $\delta \gg \gamma$ and $\delta \ll \beta$, in turn.

First, the case $\delta \gg \gamma$ is treated simply by expanding the integrand in Eq. (A1) to give

$$\begin{aligned}\rho_{bb} - \rho_{aa} &\simeq -\frac{1}{T_1}\int_{-\infty}^{t} e^{-\beta(t-t')}[1-(\gamma/\delta)(\sin\delta t - \sin\delta t')]dt' \\ &= -\frac{1}{T_1\beta} + \frac{\gamma}{2T_1}\frac{1-i\delta/\beta}{\delta^2+\beta^2} e^{i\delta t} + \frac{\gamma}{2T_1}\frac{1+i\delta/\beta}{\delta^2+\beta^2} e^{-i\delta t},\end{aligned} \tag{A2}$$

which is seen to be identical to Eqs. (12) and (13) when $-1/T_1\beta$ is recognized as the dc component $(\rho_{bb} - \rho_{aa})^{dc}$ of the inversion.

Second, the case $\delta \ll \beta$ is treated by rewriting Eq. (A1) in the form

$$\rho_{bb} - \rho_{aa} = -\frac{1}{T_1}\int_0^{\infty} e^{-\beta\tau} e^{-(\gamma/\delta)[\sin\delta t - \sin\delta t \cos\delta\tau + \cos\delta t \sin\delta\tau]} d\tau , \tag{A3}$$

where $\tau = t - t'$, and by noting that in the region of principal contribution to the integral (i.e., $\tau \lesssim 1/\beta$) we have $\delta\tau \lesssim \delta/\beta \ll 1$ and $\gamma\tau \lesssim \gamma/\beta \ll 1$. This allows us to replace $\cos\delta\tau$ by unity and $\sin\delta\tau$ by $\delta\tau$ and evaluate the resulting integral:

$$\begin{aligned}\rho_{bb} - \rho_{aa} &\simeq -\frac{1}{T_1}\int_0^{\infty} e^{-\beta\tau} e^{-\gamma\tau\cos\delta\tau} d\tau \\ &\simeq -\frac{1}{T_1}\int_0^{\infty} e^{-\beta\tau}(1-\gamma\tau\cos\delta t) d\tau \\ &= -\frac{1}{T_1\beta} + \frac{\gamma}{2T_1}\frac{1}{\beta^2} e^{i\delta t} + \frac{\gamma}{2T_1}\frac{1}{\beta^2} e^{-i\delta t},\end{aligned} \tag{A4}$$

which agrees with Eq. (A2) in the present limit $\delta \ll \beta$.

The final step in showing that Eq. (A2) is, in fact, valid for *all* values of δ is to realize that the two limiting regions of δ assumed above ($\delta \gg \gamma$ and $\delta \ll \beta$) are actually overlapping regions.

*On leave from the Norwegian Defence Research Establishment.
[1]R. Y. Chiao, P. L. Kelley, and E. Garmire, Phys. Rev. Lett. 17, 1158 (1966).
[2]R. L. Carman, R. Y. Chiao, and P. L. Kelley, Phys. Rev. Lett. 17, 1281 (1966).
[3]M. J. Pellin and J. T. Yardley, IEEE J. Quantum Electron QE-13, 904 (1977).
[4]B. R. Mollow, Phys. Rev. A 7, 1319 (1973).
[5]R. W. Hellwarth, J. Opt. Soc. Am. 67, 1 (1977); A. Yariv and D. M. Pepper, Opt. Lett. 1, 16 (1977).
[6]R. L. Abrams and R. C. Lind, Opt. Lett. 2, 94 (1978); 3, 205 (1978).
[7]J. Nilsen and A. Yariv, Appl. Opt. 18, 143 (1979).
[8]T. Fu and M. Sargent III, Opt. Lett. 4, 366 (1979).
[9]D. J. Harter and R. W. Boyd, IEEE J. Quantum Electron QE-16, 1126 (1980).
[10]B. R. Mollow, Phys. Rev. 188, 1969 (1969).
[11]F. Schuda, C. R. Stroud, Jr., and M. Hercher, J. Phys. B 7, L198 (1974).
[12]C. Cohen-Tannoudji and S. Reynaud, J. Phys. B 10, 345 (1977); 10, 365 (1977); 10, 2311 (1977); E. Courtens and A. Szöke, Phys. Rev. A 15, 1588 (1977); 17, 2119 (1978).
[13]J. L. Carlsten, A. Szöke, and M. G. Raymer, Phys. Rev. A 15, 1029 (1977).
[14]N. Bloembergen and Y.-R. Shen, Phys. Rev. 133, A37 (1964).
[15]B. R. Mollow, Phys. Rev. A 5, 2217 (1972).
[16]M. Sargent III, Phys. Rep. 43, 223 (1978).
[17]F. Y. Wu, S. Ezekiel, M. Ducloy, and B. R. Mollow, Phys. Rev. Lett. 38, 1077 (1977).
[18]J. H. Lee, J. J. Song, M. A. F. Scarparo, and M. D. Levenson, Opt. Lett. 5, 196 (1980); J. J. Song, J. H. Lee, and M. D. Levenson, Phys. Rev. A 17, 1439 (1978).
[19]N. Bloembergen, *Nonlinear Optics* (Benjamin, New York, 1965), p. 115.
[20]A. C. Tam, Phys. Rev. A 19, 1971 (1979).
[21]C. H. Skinner and P. D. Kleiber, Phys. Rev. A 21, 151 (1980).